Geomechanics and Engineering, *Vol. 34, No. 6 (2023) 623-636*
https://doi.org/10.12989/gae.2023.34.6.623

The behaviour of a strip footing resting on geosynthetics-reinforced slopes

Hamed Yazdani and Mehdi Ashtiani*

Faculty of Civil Engineering, Babol Noshirvani University of Technology, Babol, Iran

(*Received March 3, 2023, Revised July 31, 2023, Accepted August 11, 2023*)

Abstract. This study utilized small-scale physical model tests to investigate the impact of different types of geosynthetics, including geocell, planar geotextile, and wraparound geotextile, on the behaviour of strip footings placed on 0.8 m thick soil fills and backfills with a slope angle of 70°. Bearing capacity and settlement of the footing and failure mechanisms are discussed and evaluated. The results revealed that the bearing capacity of footings situated on both unreinforced and reinforced slopes increased with a greater embedment depth of the footing. For settlement ratios below 4%, the geocell reinforcement exhibited significantly higher stiffness, carrying greater loads and experiencing less settlement compared to the planar and wraparound geotextile reinforcements. However, the performance of geocell reinforcement was influenced by the number and length of the geocell layers. Increasing the geocell back length ratio from 0.44 to 0.84 significantly improved the bearing capacity of the footing located at the crest of the reinforced slope. Adequate reinforcement length, particularly for geocell, enhanced the bearing pressure of the footing and increased the stiffness of the slope, resulting in reduced deflections. Increasing the length of reinforcement also led to improved performance of the footing located on wraparound geotextile reinforced slopes. In all reinforcement cases, reducing the vertical spacing between reinforcement layers from 100 mm to 75 mm allowed the slope to withstand much greater loads.

Keywords: geocell; model tests; planar geotextile; slope-stabilization; wraparound geotextile

1. Introduction

There are many situations where foundations are located on the top of a slope (footing on an embankment and footing of a bridge abutment on sloping embankment). When a structure are constructed on sloping ground, the bearing capacity of the footing may be considerably reduced depending upon the location of the footing with respect to slope (Javankhoshdel and Bathurst 2017). Among various stabilization techniques available, reinforcing soil beneath footings by geosynthetics is a solution to improve the load-bearing capacity of footing located on the top of the slope. Use of geosynthetics has been extensively reported by researchers. These investigations have shown that both the ultimate bearing capacity and the load-settlement behaviour of the footing could be improved by the inclusion of reinforcing layers within the fill slope (Huang *et al.* 1994, Lee and Manjunath 2000, Yoo 2001, El Sawwaf 2007, Alamshahi and Hataf 2009, Choudhary *et al.* 2010, Latha 2011, Yang *et al.* 2012, Saride 2013, Turker *et al.* 2014, Khalaj *et al*. 2015, Jesmani *et al*. 2016, Won *et al.* 2016, Hedge and Sitharam 2016, Mehrjardi *et al.* 2016, Biswas and Mittal 2017, song *et al.* 2018 a, b, Kumar *et al*. 2019, Song and Tian 2019, Kazemian and Arvin 2019, Fahliani *et al.* 2021, Ardakani and Namaei 2021, Sarafrazi *et al.* 2022, Liu *et al.* 2022, Yazdani and Ashtiani 2022).

Huang *et al.* (1994) investigated the failure mechanism of reinforced sand slopes with bronze strips subjected to load on footing. They showed that the strains measured on these reinforced slopes were equal to those estimated on prototype-dimension slopes that had been reinforced with steel strips and high-stiffness geogrids. They categorized the failure mechanisms for unreinforced and reinforced slopes by considering the reinforcement length, the reinforcement position, and the vertical distance between reinforcements. The failure patterns of reinforced slopes were largely depended on the arrangements of the reinforcement layers.

Yoo (2001) experimentally and numerically investigated the bearing capacity of strip footings on geogrid-reinforced sand slopes. The results indicated that the bearing capacity of the footing increased significantly with the placement of the geogrid layers beneath the footing. The bearing capacity was controlled by the pattern of the geogrids. El Sawwaf (2007) studied the behaviour of strip footings on geogrid-reinforced sand over a soft clay slope. Partial replacement of the soft clay with a layer of sand significantly increased the bearing capacity of the footing in the vicinity of the slope crest. The reinforced sand layer increased the footing bearing load and decreased the depth of the replaced sand layer at the same settlement level.

Choudhary *et al.* (2010) conducted a small-scale experimental study to investigate the behaviour of a strip footing on a geogrid-reinforced slope with face angles of 45° and 60°. The results showed that an increase in the footing width from 100 mm to 200 mm caused a slight decrease in the bearing capacity of the footing. The bearing capacity could be improved by increasing the number of geogrid layers and the distance of the edge of the footing from the slope crest.

*Corresponding author, Assistant Professor
E-mail: m.ashtiani@nit.ac.ir

ISSN: 2005-307X (Print), 2092-6219 (Online)

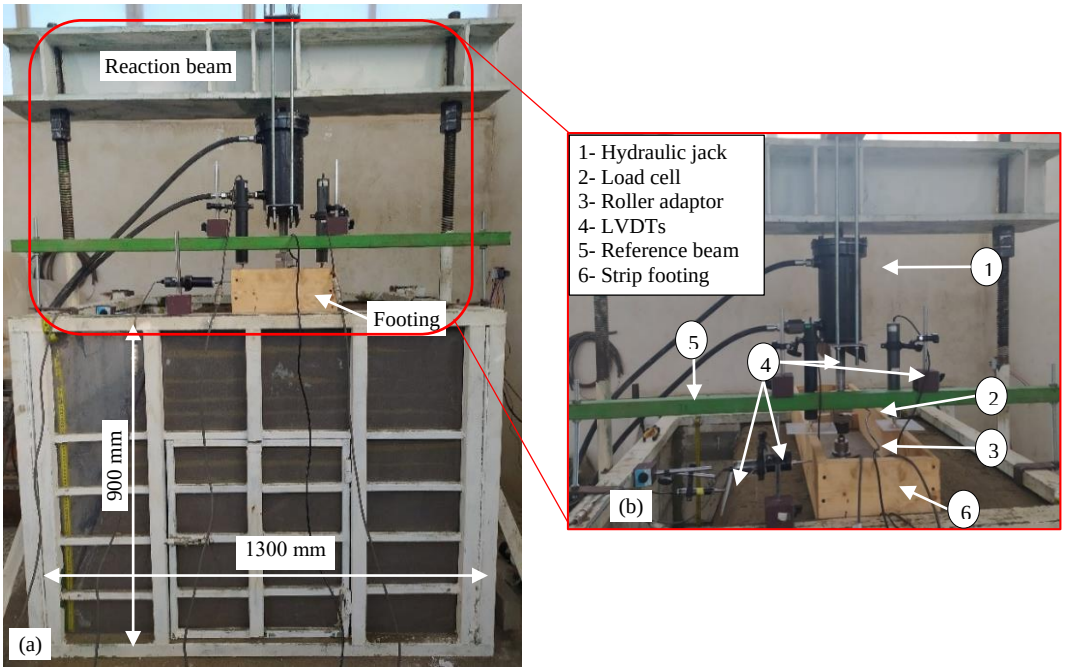

Fig. 1 Model test set-up: (a) test box with dimensions and (b) loading system and instrumentation

Mehrjardi *et al.* (2016) investigated the behaviour of a geogrid-reinforced slope with a dip angle of 45° through small-scale experimental modelling. The installation of a geogrid layer in the soil beneath the footing increased the bearing capacity of the footing in fine and coarse-grained sands compared to unreinforced slopes. Where the edge distance was less than the footing width, use length of geogrids of more than four times the footing width (B) had no significant effect on the bearing capacity of the footing. However, for an edge distance of $2B$, the use of longer geogrids improved the footing performance to some extent. In reinforced slopes, depending on the geogrid length, an increase in the distance to the edge initially increased the bearing capacity of the footing and then caused it to decrease. They further investigated failure mechanisms for reinforced slopes considering fine and coarse sand types and the reinforcement length.

Kazemian and Arvin (2019) presented a 3D numerical model of the stability of geocell-reinforced slopes using the strength reduction method. Their results showed that the installation of a geocell layer in the upper part of the slope improved the performance more than in the middle or lower parts of the slope. Fahliani *et al.* (2021) investigated the response of a strip footing resting on unreinforced and geocell-reinforced slopes using a series of small-scale modelling tests. They reported a significant improvement in the performance of the footings with the use of one geocell layer for a back length of zero. They concluded that extending the geocell length beyond the back length of zero at a smaller settlement ratio ($s/B \leq 20\%$, where s is the settlement of footing and B is the footing width), which was more than twice the footing width at $s/B \geq 20\%$, had a minor effect on the load bearing of the footing.

In most of these studies, researchers have studied the behaviour of footings situated on the reinforced slopes by planar geosynthetics or geocells separately, but there is still a lack of investigations into a comparison of planar and geocell reinforcements with regard to their benefits on the bearing capacity of footings. Also, to the author's knowledge, there is no similar study to evaluate the load-settlement behaviour of a footing supported by reinforced slope with wraparound reinforcement. Hence, in the current study, a series of small-scale experimental model tests were conducted to evaluate the effectiveness of planar geotextile, wraparound geotextile, and geocell (formed of geotextile) reinforcements on the load-settlement behaviour of a footing resting on a reinforced sand slope. These experiments were performed on a 70° slope as a steep slope composed of relatively dense, wet-compacted sandy soil.

The concept of a reinforced steep slope has been implemented with great success for various applications such as road widening and the repair of failed slopes (Yoo 2001). The purpose of experimental study was to compare the performance of the three types of reinforcement that had the same characteristics and the same reinforcement material mass. The type of failure mechanism of reinforced slopes were also examined. The parameters investigated in testing program included the vertical distance between the reinforcement layers, the length of the reinforcements, and the embedment depth of the footing. It should be noted that only one type of reinforcements, one footing width, and one type of sand were used in experimental tests.

2. Experimental program

A series of model tests were conducted inside a 1300 mm × 1100 mm × 900 mm (length × width × height) rigid testing box (Fig. 1). All sidewalls of the box were composed of smooth 8-mm-thick transparent panels to allow observation of the deformation during testing. Hollow, square steel bars were affixed to the transparent sides to

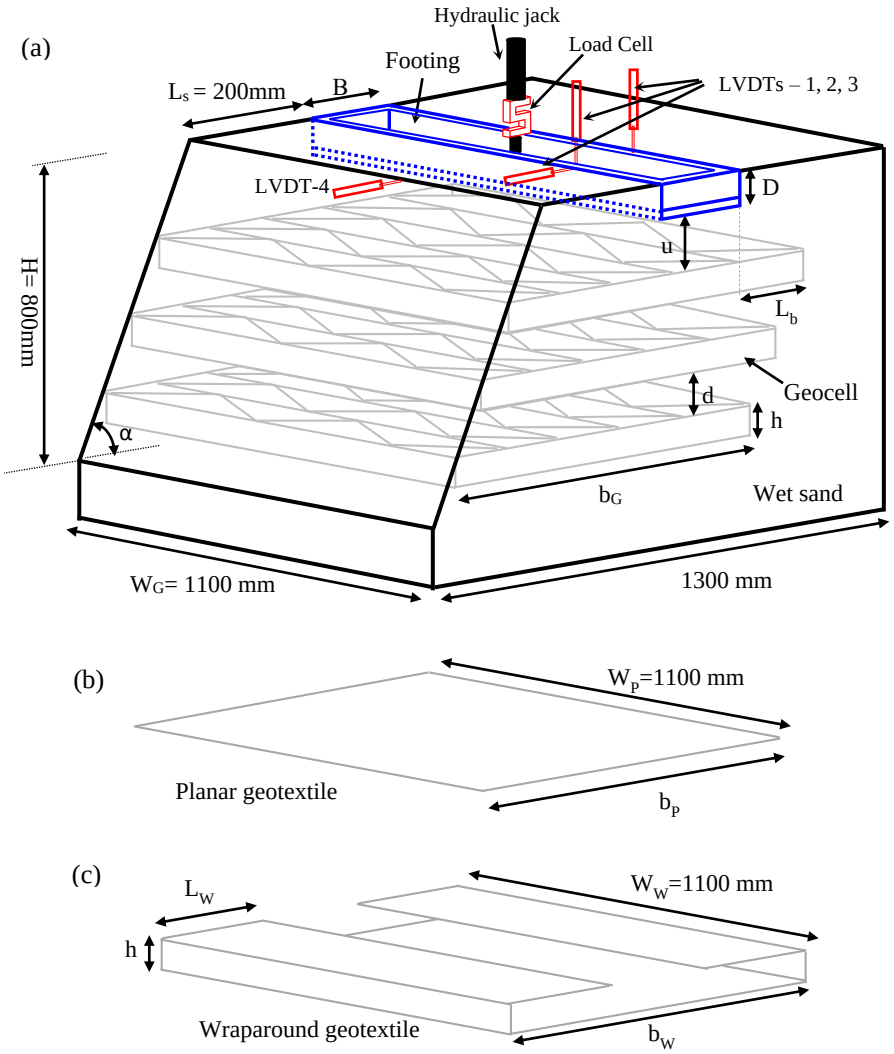

Fig. 2 Schematic of reinforced slope (not to scale): (a) Test set-up and geocell reinforced slope, (b) Characteristics of planar geotextile and (c) Characteristics of wraparound geotextile

prevent undesirable lateral deformation of the box. To minimize the boundary friction at the front and back sides of the box, silicon oil was applied to the interface between the sand and sidewalls during preparation of the model.

The box comprised the testing chamber, loading system, and data acquisition system. The loading system comprised a loading frame, 30-ton hydraulic jack, and power unit. The loading frame consisted of two circular steel columns and an I-shaped beam that supported the hydraulic jack. To avoid dependence on the loading rate in the soil-footing response, it was set at 1.0 mm/min. Both the load and displacement were automatically recorded by the data acquisition system. An S-shaped load cell with 50 kN capacity and 2.0 mV/m sensitivity was placed between the loading system and footing to measure the applied load (Fig. 1). Three linear variable displacement transducers (LVDTs) were used to monitor and measure the settlement and rotation of the footing during testing. Another LVDT was placed horizontally near the crest of the slope to record any horizontal displacement of the slope crest during testing (Fig. 1).

2.1 Problem definition

The geometry of the problem investigated in the model tests is shown in Fig. 2. Model testing was conducted on a soil slope with a height of H = 800 mm and slope angle of α = 70°. A shallow rigid footing with a breadth of B = 300 mm was placed at different embedment depths. Embedment depths D = 0 and D = 100 mm were considered as surface and shallow embedded footings, respectively. The distance between the left sidewall of the footing and the slope crest (i.e., edge length) was L_s = 200 mm. It should be noted the dimensions were chosen so that the boundary conditions have the less influence on the test results.

To evaluate the effectiveness of geosynthetics reinforcements on the behaviour of the footings resting on the soil slope, geocell layers of length b_G, width W_G, height h, and spacing d were placed at the depth of the top of the first geocell layer beneath the footing base u (Fig. 2(a)). For the planar-geotextile reinforced slope (Fig. 2(b)), the geotextile layers used had length b_P and width W_P. For the wraparound-geotextile reinforced slope (Fig. 2(c)), the tests were conducted using wraparound geotextile layers of

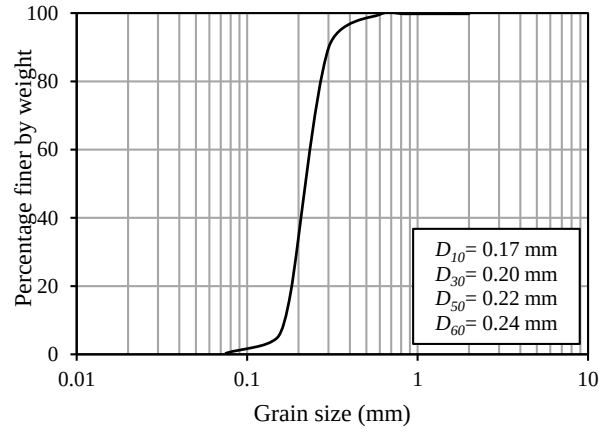

(a) Particle size distribution curve of test sand

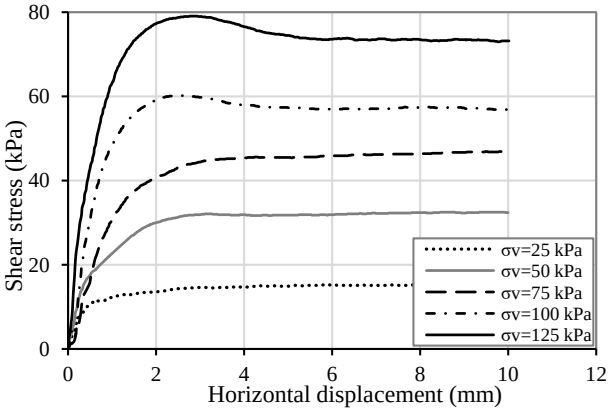

(b) Direct shear test results of the sand

Fig. 3 Soil used in the model tests

Table 1 Properties of sand used in model tests

Description	Value
Medium grain size, D_{50} (mm)	0.22
Minimum void ratio, e_{min}	0.57
Maximum void ratio, e_{max}	0.81
Relative density, D_r (%)	60
Specific gravity, G_s	2.79
Peak friction angle, φ_P (°)	32
Residual friction angle, φ_r (°)	29
Dilation angle, ψ (°)	4

length b_W, height h, width W_W, and lap length L_W. The width of all geosynthetics reinforcements is 1100 mm. All dimensions are presented at model scale unless stated otherwise.

2.2 Materials used for testing

2.2.1 Soil

The soil used was uniform sand classified as SP according to the Unified Soil Classification System, with the properties of D_{10} = 0.17 mm, D_{50} = 0.22 mm, C_u = 1.39, C_c = 0.97, e_{max} = 0.81, and e_{min} = 0.57. Fig. 3(a) shows the grain-size distribution curve of the sand. All tests were carried out at a relative density (Dr) of 60% (corresponding to a unit weight of 16.4 kN/m^3) and a moisture content of 5%. The friction and dilation angles were determined by direct shear test at normal stresses ranging from 25 kPa to 125 kPa (see Fig. 3(b)). The properties of the sand used in the model tests are summarized in Table 1.

Table 2 Properties of model reinforcement materials

Description	Geotextile	Geocell
Type	Non-woven	Non-woven geotextile
Mass per unit area (g/m^2)	80	-
Thickness, (mm)	0.23	0.23
Tensile strength (kN/m)	1.4	1.4
Strength at 5% (kN/m)	0.48	0.48
Junction strength (kN/m)	-	1.52

2.2.2 Reinforcements

Non-woven polypropylene geotextile was used to make the geocell and wraparound geotextile. The geotextile was chosen to have a low tensile strength to model the prototype material. The tensile strength of a geotextile sample of 50 mm in width was 1.4 kN/m at the model scale (based on ASTM D4595). The tensile test results for the non-woven geotextile are shown in Fig. 4. Table 2 summarizes the geotextile and the geocell properties.

The geocell were made from non-woven geotextile strips glued together to form a honeycomb pattern with cross-diagonal members and an open top and bottom. To evaluate the seam strength of the geocell, force was applied at the two ends of the sample at the junction until the seam failed (Chen and Chiu 2008). The junction strength of the geocell was 1.52 kN/m (Table 2). The opening size and the height of the geocell were both 50 mm and were kept constant in all tests.

2.3 Scale effect

The model-scale slope was designed based on a target scaling factor of SF = 10. To ensure comparable behaviour between the model-scale and prototype-scale slopes, the tensile strength of the geotextile material was scaled down using a scaling factor of 1/SF^2 (Viswanadham and König 2004, Chen and Chiu 2008). The geotextile material for the model tests was selected to be as thin as possible and exhibited low tensile strength to determine the correct response of the prototype-scale slope. The tensile strength of the geotextile and geocell was 1.4 kN/m at model scale. This corresponds to reinforcement with a tensile strength of 140 kN/m at prototype scale, which falls within the range of the tensile strength of commercial reinforcements. The scaling between the model-scale and prototype-scale slopes was 1/10 for the linear dimensions (footing and reinforcement dimensions, soil depth, and displacement).

As stated before, the opening size and the height of the geocell were both 50mm. Therefore, the opening size and the height of the geocell would be 0.5 m for the prototype-scale slopes. Although, these values would not be within the range of commercial geocells, preparing the models with smaller opening sizes and heights was very difficult. It should be noted, the opening size and the height of geocell

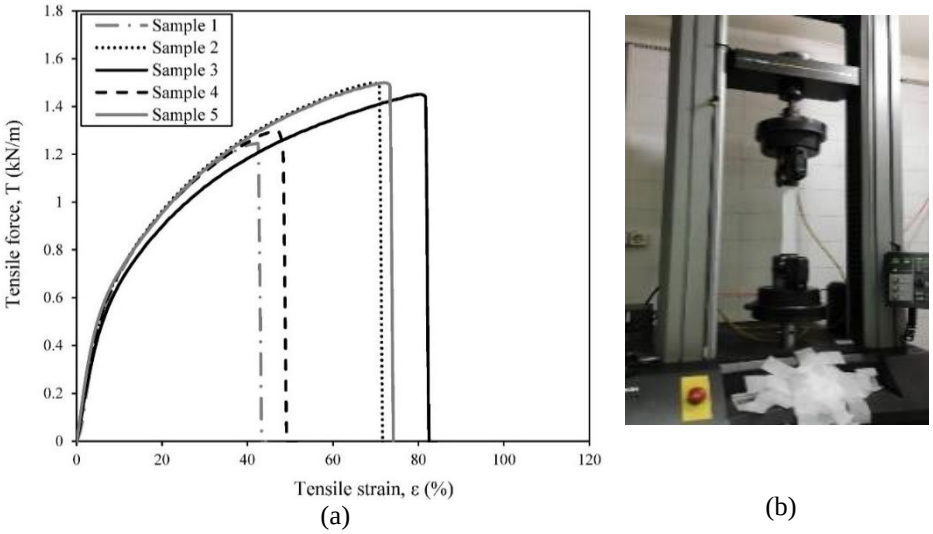

Fig. 4 Wide-width tensile test results for non-woven geotextile; (a) the tensile load-strain response and (b) image of test

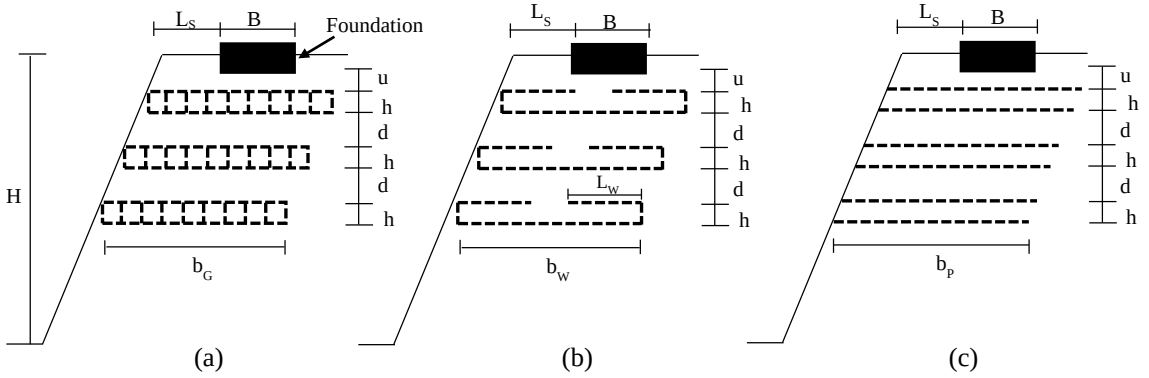

Fig. 5 Arrangement of reinforced slopes (not to scale) for: (a) geocell, (b) wraparound geotextile and (c) planar geotextile

significantly influence the equivalent stiffness of the geocell-soil composite between the model-scale and prototype-scale slopes (Latha *et al.* 2008, 2009, Song *et al.* 2020, 2022).

2.4 Testing program

A total of 14 model slopes with 0.8 m high and 70° slope using different reinforcement materials, reinforcement positions and lengths, and footing embedment depths were constructed inside the test box. Fig. 5 shows the details of the arrangements of the reinforcements in the model tests. The variables for the model tests were:

- Reinforcement type: geocell, planar geotextile, wraparound geotextile
- Spacing of reinforcement (d): 75 mm, 100 mm
- Lengths of reinforcements (b_G, b_P, b_W): 650 mm, 700 mm, 770 mm, 870 mm
- Embedment depths of footing D : 0 mm, 100 mm

Table 3 lists the characteristics of the model tests. These values were kept constant in all tests. The position of the first layer of reinforcement below the footing base was u = 50 mm, the height of reinforcement was h = 50 mm, and the edge length of the footing (distance between the left corner of the footing and the slope crest) was L_S = 200 mm.

According to Tafreshi and Dawson (2010), to ensure comparable behaviour for the effectiveness of the reinforcement types on the bearing capacity of the footing resting on a geosynthetics-reinforced slope, the quantity of reinforcing material (mass per unit area) must be the same in all model tests. This value is a function of the number of layers, their length, height, and spacing, as well as the lap length for the wraparound geotextile. In this regard, a geocell layer with a height of h = 50 mm, a cell size of 50 mm, and a length b_G of 650 mm is equivalent to two planar geotextile layers of length b_P = 700 mm. This is equivalent to a wraparound geotextile layer of height h = 50 mm, length b_W = 700 mm, and lap length L_W = 290 mm. Similarly, a geocell layer of height h = 50 mm and length b_G = 770 mm is equivalent to two planar geotextile layers of length b_P = 870 mm and to a wraparound geotextile layer of height h = 50 mm, length b_W = 870 mm, and lap length L_W = 380 mm. For the geocell with h = 50 mm, two geotextile layers were placed at the top and bottom of the geocell layer (Figs. 5(a) and 5(c)).

Table 3 Summary of model tests

Test no.	Type of reinforcement	N	b_G, b_W or b_P (mm)	L_W (mm)	d (mm)	D (mm)	Reason
1	Ur	-	-	-	-	0	Effect of reinforcement type and spacing between reinforcements
2	GC	3	650	-	75	0	
3	GT	6	700	-	75	0	
4	WGT	3	700	290	75	0	
5	GC	3	650	-	100	0	
6	GT	6	700	-	100	0	
7	WGT	3	700	290	100	0	
8	Ur	-	-	-	-	100	Effect of embedment depth of footing
9	GC	3	650	-	75	100	
10	GT	6	700	-	75	100	
11	WGT	3	700	290	75	100	
12	GC	3	770	-	75	0	Effect of reinforcement length
13	GT	6	870	-	75	0	
14	WGT	3	870	380	75	0	

N: number of reinforcement layers; b_G, b_W, b_P: length of reinforcements; L_W: Lap length; d: Spacing of reinforcements;
D: embedment depth of footing
Ur: unreinforced; GC: geocell; GT: planar geotextile; WGT: wraparound geotextile

2.4.1 Selecting test parameters

The reason for choosing a slope with a face angle of 70° was to investigate the behaviour of the slope at a steep face angle and also because space limitations in the test box minimized the boundary effects of the walls. Previous studies have revealed that, to prevent local buckling in the geocell walls below the footing, the first layer of geocell should be placed at $u/B \geq 0.1$, where u is the depth of the first geocell layer, and B is the width of the footing (Dash *et al.* 2007). Thus, in the present study, this ratio was selected to be 0.17 for reinforced slopes. In order to compare the behaviour of the reinforced slopes, this parameter was kept constant for other reinforcements as well.

Michalowski (1997) used the results of limit analysis to show that, in order to prevent slope failure as a result of rupture, pull-out, or direct sliding of the reinforcement, the length of the reinforcement should be 0.65 times the height of the slope. Viswanadham and König (2009) used a geotechnical centrifuge to study the behaviour of geotextile-reinforced slopes subjected to non-uniform settlement and reported that the constant length of the reinforcement should be 0.85 times the height of the slope. Even after inducing non-uniform settlement equivalent to 1.0 m in prototype dimensions, the geotextile-reinforced slope did not experience collapse. Therefore, the length of the geocell reinforcement in the current research was selected as 650 mm (0.81 times the height of the slope).

Sharma *et al.* (2009) analytically estimated the ultimate bearing capacity of a footing on geogrid reinforced soil for both sandy and clay-layered soils. They reported that the vertical distance between the reinforcing layers should be less than $0.5B$ to avoid failure in the actual design. El Sawwaf (2007) showed that, in order to achieve maximum improvement in the bearing capacity of a footing, the vertical distance between the reinforcements should be $0.5B$. Yoo (2001) and Alamshahi and Hataf (2009) proposed a similar trend for sand slopes and found that the critical value for the vertical distance between reinforcements should be in the range of $0.7B$ to $0.75B$. In the current study, for a footing width of 300 mm, the vertical distances between the reinforcements were selected as 75 and 100 mm (i.e., less than $0.5B$).

Yazdani and Ashtiani (2022) found that, in order to increase the bearing capacity of a footing resting on a reinforced slope with a high face angle ($\alpha = 70°$), a minimum number of reinforcing layers is required. They reported that at least three layers of geocell are required and, if this number of reinforcing layers is not used, the bearing capacity of footing placed on the reinforced slope will not change compared to that of the unreinforced case.

In the present study, the number of reinforcement layers was kept constant at three to enable comparison of the effect of different reinforcements. It should be noted that the footing width, footing distance from the slope crest, and relative density of the sand, were held constant in all tests. Therefore, the results of this study may differ from the results at prototype scale and more model tests are required to achieve more comprehensive results

2.4.2 Model preparation

The soil for model testing was prepared using the wet tamping method (Ashtiani *et al.* 2015). In preparation for testing, the sand layers were subdivided into 50-mm thick layers and each was compacted to a dry density of 16.4 kN/m3 at a moisture content of 5%. The sand was compacted through a pre-calibrated steel tamping hammer to maintain the relative density of the soil at 60%.

Using the planar geotextile reinforcement technique, as the sand layer reached the level of the first geotextile layer, this layer of reinforcement was placed on the soil surface. After that, soil compaction was continued until the desired levels for the other layers of geotextile were achieved. For the wraparound geotextile reinforcement technique, the wraparound geotextile layers similarly were placed at the desired depths. The sand above the planar section of the geotextile and around the wraparounds laps was compacted

using a steel hammer. After that, the geotextile was lapped over the compacted sand layer. Soil compaction was continued up to the desired levels for the other wraparound geotextile layers. For geocell reinforcement, as the sand layer reached the first geocell level, the first layer of reinforcement was placed on the sand surface (see Fig. 6). After that, the cell pockets were compacted using a small steel hammer and soil compaction continued up to the footing base level. All reinforcement layers were prepared having a width equal to the entire length of the test box.

When the sand layer reached the footing base level, the footing was placed at its designated position. The rest of the sand layer was compacted to obtain the desired model height after installation of the footing. After completion of the model, a trench having the desired facing angle was excavated to prepare the slope model.

3. Results and discussion

As the goal of this study was to evaluate the effect of geosynthetics reinforcement types on the bearing capacity of a footing located on a soil slope, the results of the reinforced slopes compared to the unreinforced slope have been presented. The effect of different reinforcement types also has been investigated. For this purpose, an initial comparison was made between the bearing capacity of the footing and the horizontal displacement of the slope crest using the different reinforcements. The parameters of the embedment depth of the footing, the reinforcement length, and the spacing between the reinforcements were examined.

The performance of the different reinforcements was then investigated using the bearing capacity ratio (BCR = q_r/q_{ur}), where q_r is the bearing capacity of the footing on a reinforced slope and q_{ur} is the bearing capacity of the footing on an unreinforced slope at the same settlement ratio. The settlement ratio of the footing equals that for the footing settlement to footing width (s/B). The failure mechanisms of the footing on the slope reinforced with different reinforcements also were determined.

3.1 Embedment depth effect

Fig. 7 shows the load-settlement graphs for the footing located on slopes reinforced with geocell, planar geotextile, and wraparound geotextile at embedment depths of $D = 0$ as surface footing and D = 100 mm as embedded one. As stated, the total mass of the reinforcement layers used was the same. To determine the impact of the reinforcements, two tests initially were conducted on footings with embedment depths of D = 0 and 100 mm placed on unreinforced slopes. The peaks of the load-settlement graphs were considered as the ultimate bearing capacity of the footing. However, as shown in Fig. 7, there was no peak point to be considered as the ultimate bearing capacity for the wraparound-geotextile reinforced slope with an embedment depth of D = 0. Thus, the ultimate bearing capacity was determined using the double-tangent method proposed by Adams and Collin (1997).

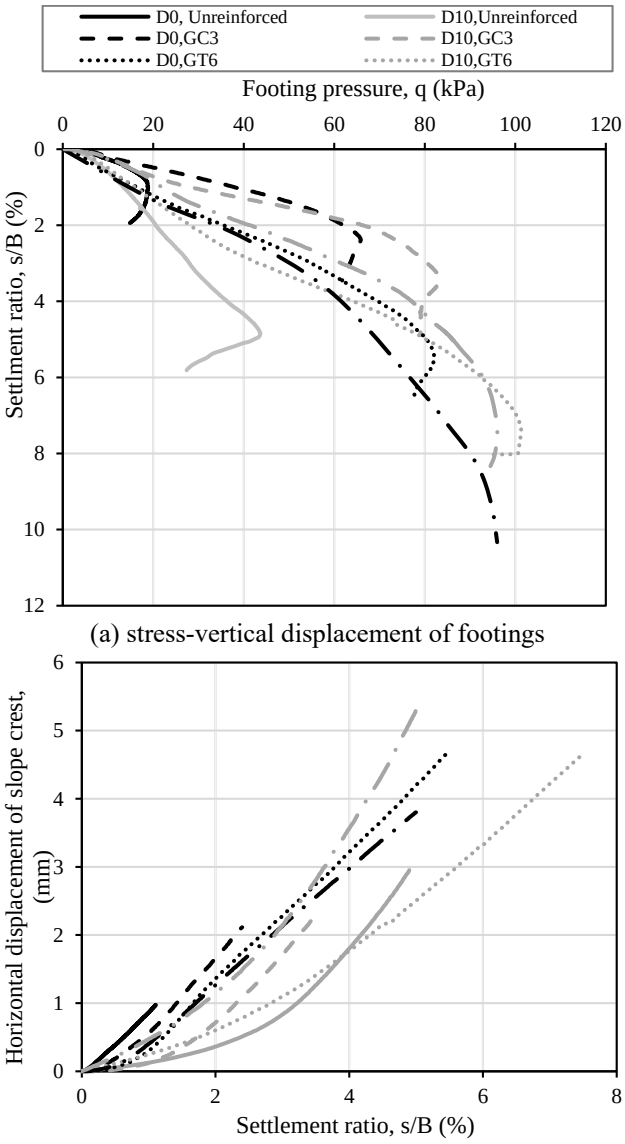

(a) stress-vertical displacement of footings

(b) horizontal displacement of slope crest

Fig. 7 Effect of embedment depth on behaviour of footing and slope reinforced with geocell, planar geotextile and wraparound geotextile

Fig. 7(a) shows that an increase in the embedment depth of the footing increased its load-bearing capacity (i.e. bearing pressure at a given settlement). For unreinforced slopes, the ultimate bearing capacity of the surface and embedded footings were 18 kPa and 43 kPa, respectively. The improvement ratio of the ultimate bearing capacity was 58% resulting from embedding the footing at D = 0 to D = 100 mm. Also, the increase in the bearing capacity of the footing at D = 100 mm compared to the surface footing for the slopes reinforced with geocell, planar geotextile, and wraparound geotextile were 27%, 23%, and 38%, respectively.

The increase in the bearing capacity of the embedded footing could be attributed to a change in the passive resistance failure zone beneath the footing. It is clear that an increase in the embedment depth of the footing increased the passive resistance failure zone beneath the footing. As a

result, the bearing capacity of the footing increased. The reinforcement lengths for both $D = 0$ and $D = 100$ mm were kept constant; thus, an increase in the embedment depth of the footing slightly decreased the back length of the reinforcement (L_b in Fig. 2) with regard to the surface footing. The L_b/B ratio corresponding to the first layer of geocell reinforcement beneath the surface and the embedded footing were 0.44 and 0.24, respectively. As can be seen, an increase in the embedment depth of the footing caused a decrease in the anchorage length of the reinforcement beyond the failure wedge. However, an increase in the embedment depth also increased the bearing capacity of the footing.

Fig. 7(b) shows the increasing horizontal displacement of the slope crest with an increase in the settlement ratio of the footing. The results show that, at a constant settlement ratio, an increase in the embedment depth of the footing caused a decreasing trend in the displacement of the slope crest for all types of the reinforcement. This could also be attributed to extension of the passive resistance zone, which increased the stiffness of the reinforced slope. Furthermore, with an increase in the embedment depth, the footing experienced greater settlement.

Fig. 8 shows the bearing capacity ratio (BCR) versus the settlement ratio for footings at embedment depths of $D = 0$ and $D = 100$ mm. As stated, the ultimate bearing capacity increased significantly with an increase in embedment depth of the footing (Fig. 7(a)). Under these conditions, the BCR of the footing also was greater than one in all cases. Fig. 8 shows that, for a footing at $D = 100$ mm and geocell as the reinforcement (i.e., test D10,GC3), the BCR decreased. This could be attributed to two factors including an increase in the bearing capacity of the footing with an increase in the embedment depth and a decrease in the back length of the reinforcements (anchorage length). For the unreinforced case, an increase in the embedment depth of the footing increased the bearing capacity. However, at a constant reinforcement length, an increase in the embedment depth of the footing caused a decrease in the anchorage length of the embedded footing. Thus, the bearing capacity of the embedded footing did not experience a significant increase.

At small settlement ratios, i.e., $s/B < 4\%$, the BCR of the geocell reinforcements for both surface and embedded footings were greater than the two other reinforcements. With an increase in the settlement ratio, the planar and wraparound geotextiles recorded higher BCR values than the geocell. The geocell-soil composite may behave as a rigid slab (Pokharel *et al.* 2010, Tang and Yan 2013), which could lead to distribution of the applied load over a wider area. The effect of the type of membrane and the distribution of the vertical stresses (Zhang *et al.* 2009) caused a large portion of the applied load on the slope to be transferred to greater depths and initiated the deep footing mechanism (Huang *et al.* 1994, Lee and Manjunath 2000).

As the number of geocell layers was kept constant as three, the failure zone developed under the last layer of geocell as a deep-footing mechanism. Therefore, for slopes reinforced by multi-layered geocell layers in the entire height of the slope, the geocell layers prevent the development of the failure plane beneath the last layer of the geocell. Also, they improve the load-bearing capacity of the footing located on the reinforced slope.

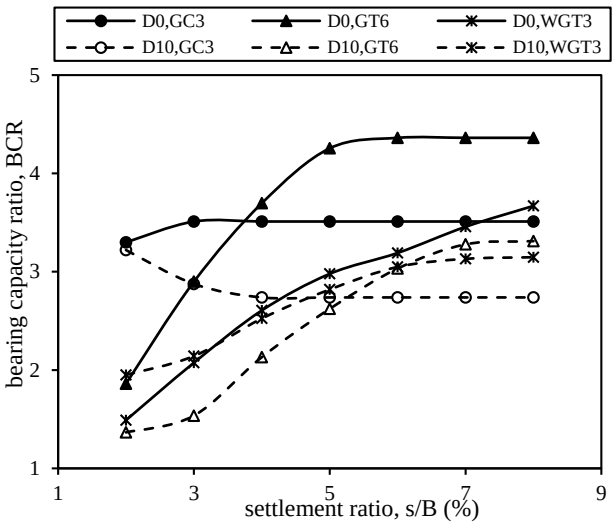

Fig. 8 BCR of strip footings resting on reinforced slopes vs. embedment depth for geocell, planar geotextile, and wraparound geotextile reinforcements

It should be noted that the back length of the geocell was much smaller than that of the planar and wraparound geotextiles. For surface footing, the back length (L_b/B) of the geocell and the two other reinforcements were 0.44 and 0.61, respectively. For embedded footing, $L_b/B = 0.26$ and $L_b/B = 0.42$ were for the geocell and the two other reinforcements, respectively. Under these conditions, an increase in the settlement ratio did not generate a large strain at the anchorage length of the geocell. Thus, failure of slope occurred more rapidly. In this case, the planar geotextile exhibited better performance than the wraparound geotextile and the geocell reinforcements. Although, it can be seen in Fig. 5, the footing experienced relatively large displacement for slopes reinforced with the planar geotextile.

Fig. 9 presents the performance of different reinforcements versus the footing settlement ratios for two embedment depths (D= 0, 100 mm). The geocell exhibited better performance at small settlement ratios. But, by increasing the settlement ratio, the planar geotextile represented better performance than the two other reinforcement types.

3.2 Reinforcement length effect

The effect of the reinforcement length on the bearing capacity of a strip footing was investigated at different geosynthetics reinforcement lengths. As stated, all other conditions were kept constant for the different reinforcements by using the same total mass. The lengths of the other two reinforcements were determined for geocell lengths of 650 and 770 mm. These lengths were equivalent to planar and wraparound geotextile layer lengths of 770 and 870 mm, respectively. Table 3 lists the reinforcement dimensions.

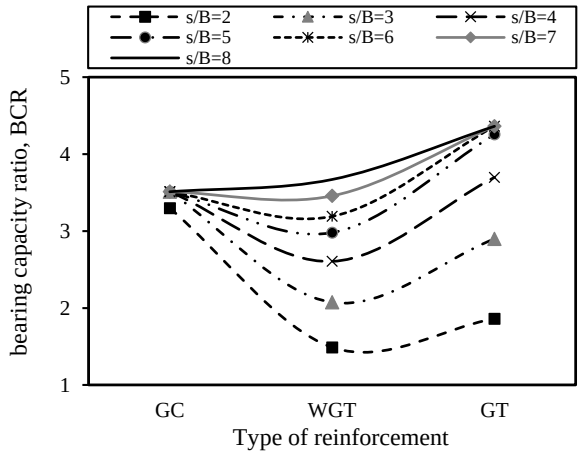

(a) Surface footing, $D = 0$

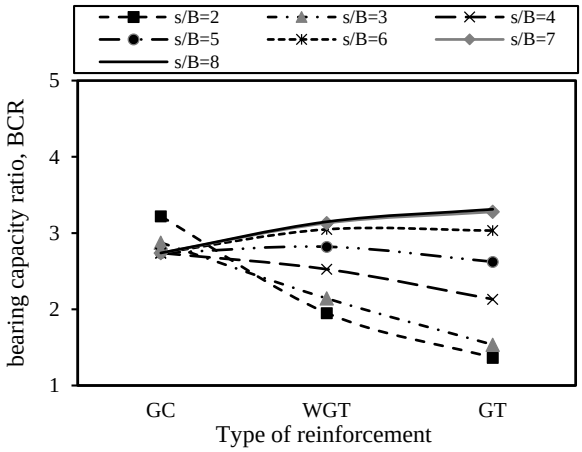

(b) Embedded footing, D = 100 mm

Fig. 9 Performance of different reinforcements on the BCR of footings vs. embedment depth

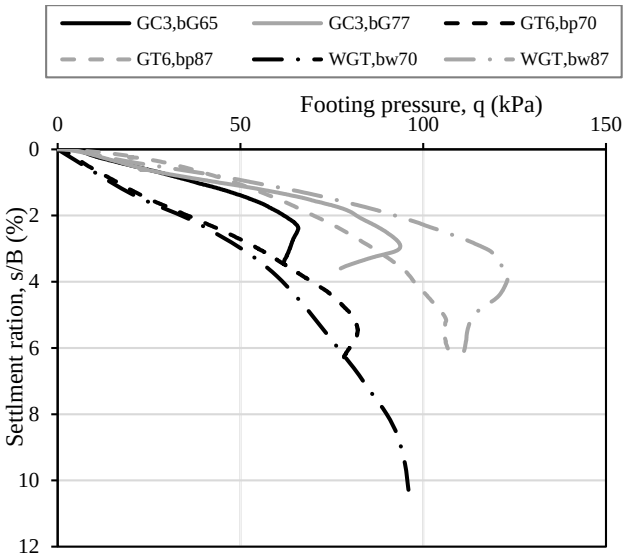

(a) Stress-vertical displacement of footings

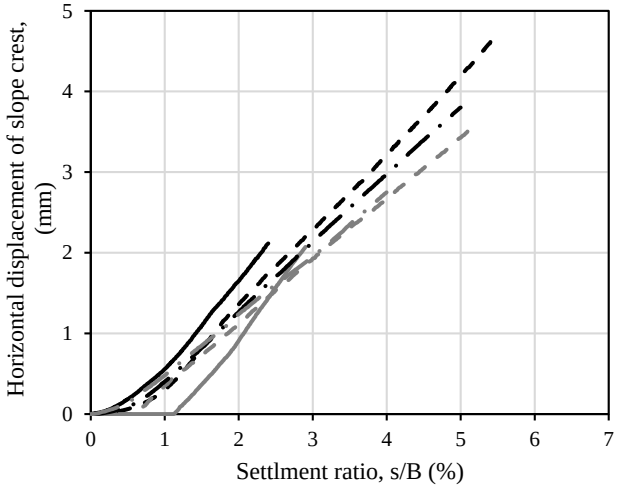

(b) Horizontal displacement of slope crest

Fig. 10 Effect of length of reinforcement layers on the behaviour of footing and slope reinforced with geocell, planar geotextile, and wraparound geotextile

Fig. 10(a) shows the load settlement for a strip footing located on a reinforced sand slope. The results show that the bearing capacity of the footing increased with an increase in the reinforcement length for all types of reinforcement. As the reinforcement length increased, the bearing capacity increased by 31%, 76%, and 23% for geocell, wraparound geotextile, and planar geotextile, respectively. These values show that the reinforcement efficiency is strongly associated with the reinforcement length. In addition, an increase in the reinforcement length produced a larger and deeper failure zone, resulting in a larger bearing capacity. The increase in the bearing capacity of the footing and the change in the failure mechanism of the reinforced slope could be attributed to the increase in the anchorage length of the reinforcement beyond the failure zone of the slope in the passive zone.

Fig. 10(b) shows the horizontal displacement of the slope crest with respect to the settlement ratio for a strip footing on a reinforced sand slope. It can be inferred that the greatest decrease in the horizontal displacement of the slope crest occurred with an increase in the geocell length. In other words, the geocell contributed considerably more to the increase in the stiffness of the reinforced slope compared to the two other reinforcements. It was noted that the increase in the shear strength in the soil-reinforcement interface and the geocell-induced stiffness tended to limit horizontal displacement of the slope. The increase in length of the other reinforcements also increased the stiffness of the slope, which attenuated horizontal displacement of the slope crest.

Yoo (2001) and Fahliani *et al.* (2021) showed that, at $L_b/B \geq 0$, the L_b/B ratio had no significant effect on the bearing capacity of the footing for a slope reinforced with either geogrid or geocell at a maximum face angle of 35°. Thus, creating no significant strain in the back length of the reinforcement. However, the results of this study show that, at $L_b/B = 0.44$ (i.e., short geocell) and $L_b/B = 0.84$ (i.e., long geocell), the bearing capacity of the footing changed significantly. This difference can be attributed to the difference in the angle of the slope face and the type of soil.

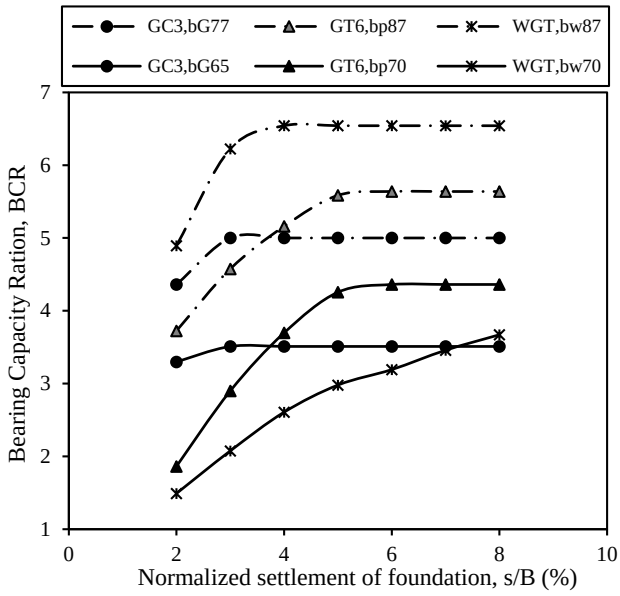

Fig. 11 Bearing capacity ratio of different lengths of reinforcement layers in regard to the normalized settlement of footing

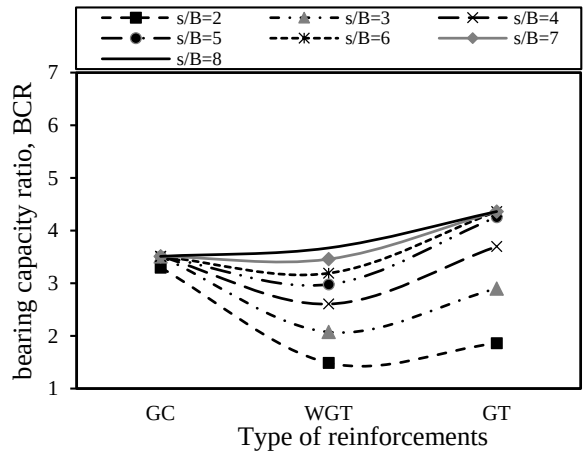

(a) Shorter reinforcements

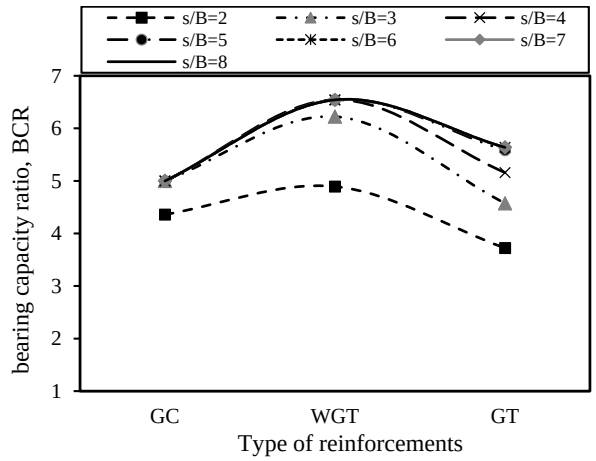

(b) Longer reinforcements

Fig. 12 Performance of different lengths of reinforcements on the BCR of the footing

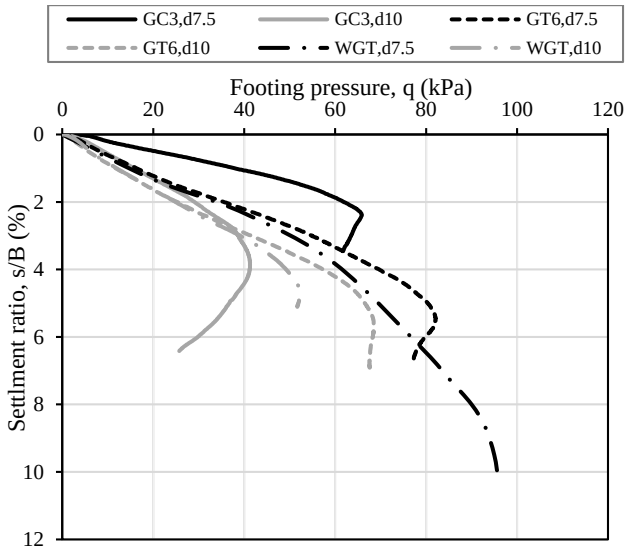

Fig. 13 Effect of spacing of reinforcement layers on the load-settlement of footing

In the present study, the model tests were conducted for slopes with a face angle of 70°, which largely affected the failure mechanisms of the unreinforced and reinforced slopes

3.3 Reinforcement spacing effect

Fig. 13 shows the effect of the vertical distance between reinforcements on the load–settlement behaviour of a strip footing located on a reinforced slope. The results show a significant decrease in the bearing capacity with an increase in the reinforcement spacing from 75 to 100 mm. This could be attributed to a change in the failure mechanism. As the reinforcement spacing increased, displacement of the soil surrounded by two reinforcements increased, resulting in the possibility of shear failure formation in the zones between the reinforcement layers (in this case, between the second and third layers). However, failure surface of the reinforced slope occurred beneath the last layer of reinforcement when the reinforcement spacing was sufficiently small.

Fig. 14 shows the BCR with respect to the settlement ratios for reinforcement spacings of 75 mm and 100 mm. At 75 mm, the geocell exhibited better performance than the other reinforcements at lower settlement ratios ($s/B \leq 4\%$). However, as the settlement ratio increased, the planar and wraparound geotextile reinforcements represented better performance than the geocell. An increase in the settlement ratio caused the stress to be distributed in the zone beneath the last layer of geocell reinforcement and the failure surface occurred in this zone. Moreover, at all settlement ratios, all reinforcements exhibited better performance for a reinforcement spacing of 75 mm than it was for 100 mm.

This could be attributed to the decrease in stiffness of the reinforced slope with an increase in the reinforcement spacing, which increased the probability of failure propagation between the reinforcement layers. This can be observed in Fig. 15, which depicts the performance of the

Table 4 Summary of failure mechanisms of geosynthetics-reinforced slopes

Type of Reinforcement	Reinforcement spacing, d= 75mm			Reinforcement spacing, d= 100mm		
	s/B< 3%	3% <s/B< 4%	s/B> 4%	s/B< 3%	3% <s/B< 4%	s/B> 4%
Geocell	No failure	Local Failure		No failure	- Local Failure - Non-persistent tension cracks	
Wraparound geotextile	No failure	- Local Failure - External failure - Non-persistent cracks		No failure		- Local Failure - External failure - Non-persistent cracks
Planar geotextile	No failure		- Internal Failure - External failure - Persistent cracks	No failure		- Internal Failure - External failure - Persistent cracks

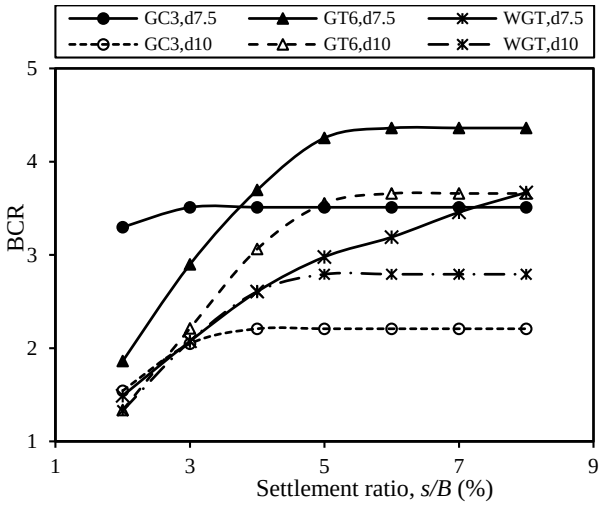

Fig. 14 BCR at different reinforcement spacings vs. the settlement ratio of the footing

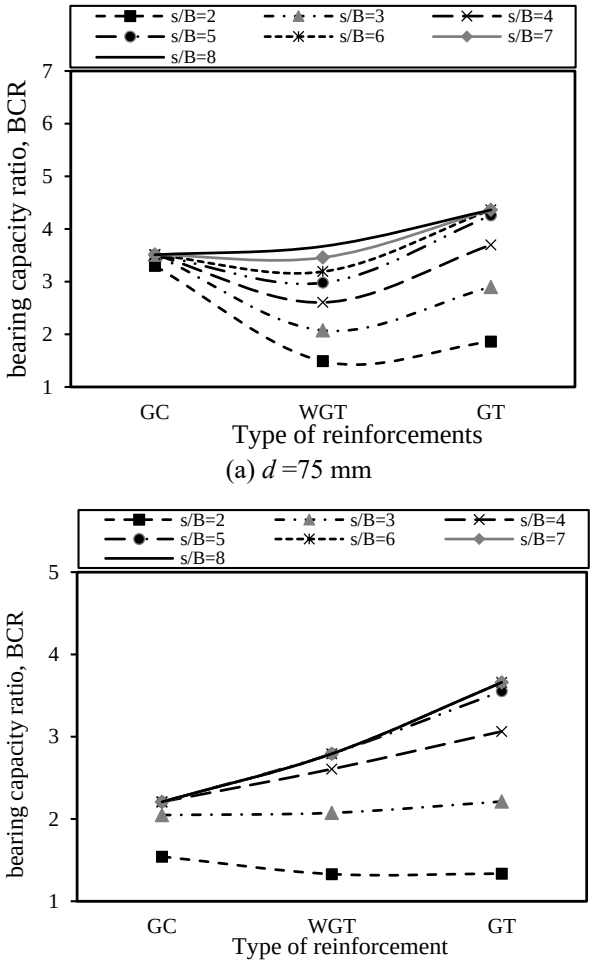

Fig. 15 Performance of different reinforcements vs. BCR of footing for different reinforcement spacings

different reinforcements with respect to their settlement ratios at 75- and 100-mm reinforcement spacings. With an increase in the reinforcement spacing to 100 mm, the planar geotextile represented better performance than the other reinforcements at greater settlement ratios ($s/B \geq 4$). Nevertheless, as shown in Fig. 12, the wraparound geotextile exhibited better performance when the reinforcement length increased.

3.4 Failure mechanisms

Small-scale physical modelling of the sandy slopes indicated that geosynthetics reinforcements can significantly improve the bearing capacity of a footing located on a slope. The practical role of reinforcements in increasing the bearing capacity shows that different failure mechanisms may form for both the unreinforced and reinforced slopes. The failure mechanisms of the slope models were studied according to the responses of the footings to the applied loads and by observation of the deformation of the soil and reinforcement layers during testing. Both the load-settlement behaviour and the shape of the failure surface of the slopes reinforced with different arrangements of reinforcement layers had significant effects on the failure mechanisms.

Fig. 16 and Table 4 show the failure mechanisms for unreinforced and reinforced slopes at reinforcement spacings of 75 mm and 100 mm. For the unreinforced slope, failure occurred at the top of the slope shortly after the onset of loading. This type of mechanism manifested as sudden and complete failure of the slope (Fig. 16(a)). For geocell-reinforced slope models (Figs. 16(b) and 16(c)), a quasi-rigid zone developed beneath the foundation. The effect of the geocell membrane caused the load to be distributed directly beneath the last layer and generated a local failure mechanism (deep-footing mechanism). For a geocell-reinforced slope with a spacing of 75 mm, the rupture propagation started under the last layer and reached

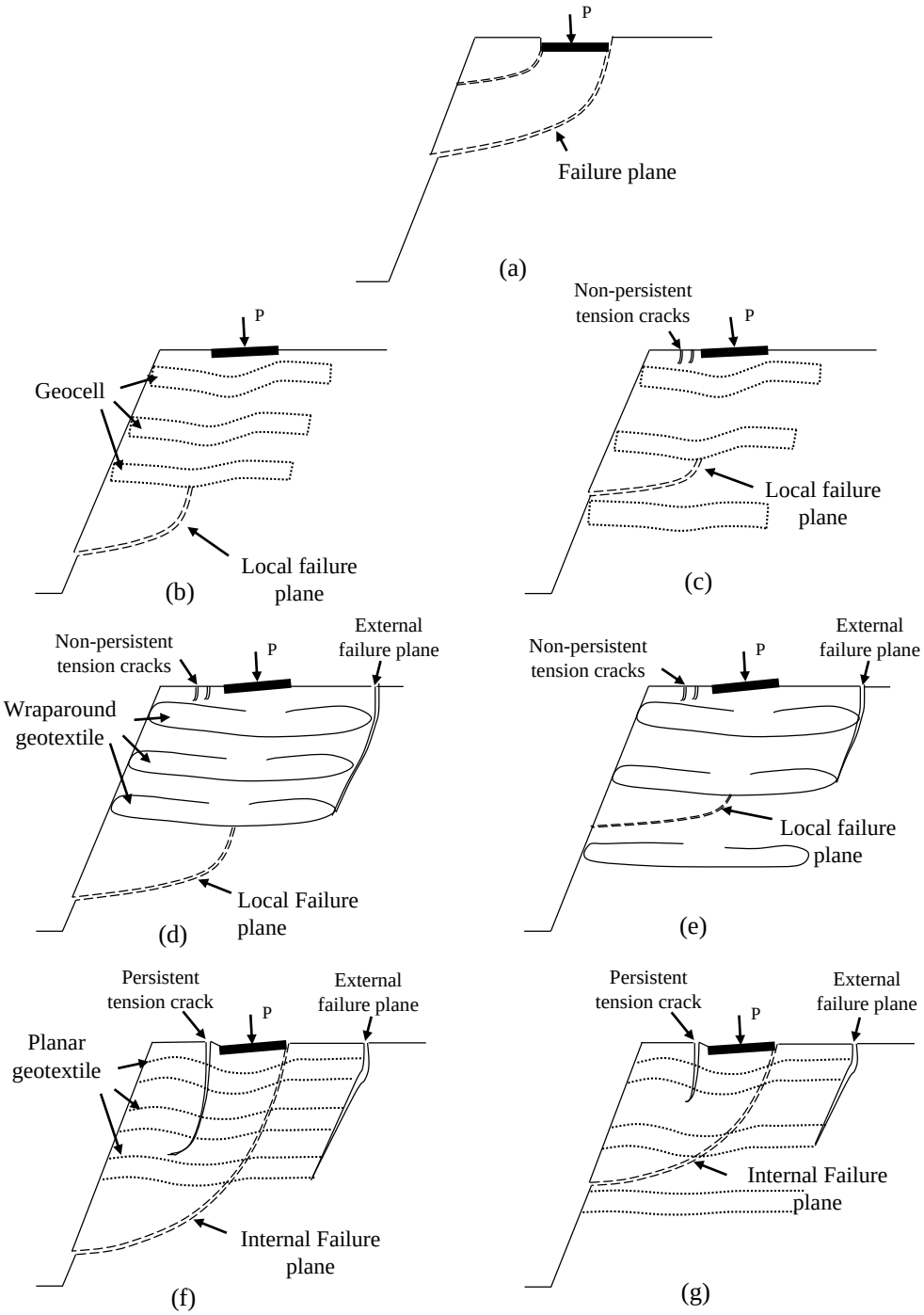

Fig. 16 Schematic failure mechanisms for: (a) unreinforced slope; (b), (d), (f) reinforced slopes with 75-mm spacing; (c), (e), (g) reinforced slopes with 100-mm spacing

the slope face. For a spacing of 100 mm, the failure shifted slightly upward and propagated beneath the second geocell layer. Almost no tensile cracks were observed on the slope face.

Figs. 16(d) and 16(e) show the same mechanism for the wraparound-geotextile reinforced slopes. In addition to local failure, a series of tensile cracks (non-persistent cracks between the footing and slope crest) and an external failure plane (persistent slip surface on the right side of the footing) have been observed. Generally, the wraparound-geotextile reinforced slopes exhibited less stiffness than the geocell-reinforced slopes, which experienced relatively more deformation.

The failure mechanisms of the planar geotextile-reinforced slopes differed. The critical slip surface intersected all the reinforcement layers to generate internal failure mechanisms. Figs. 16(f) and 16(g) show wider tensile cracks on the planar geotextile-reinforced slopes than on the wraparound-geotextile reinforced slopes. The planar-geotextile reinforced slopes also experienced much larger deformations than the other reinforcements.

4. Conclusions

An experimental investigation was performed on the behaviour of strip footings resting on unreinforced and reinforced sand slopes at a face angle of 70°. Small-scale laboratory model tests were conducted and the vertical load was applied to the strip footing with 1.0 mm/min loading rate. The effects of geocell, planar-geotextile, and wraparound-geotextile reinforcements were investigated. The purpose of experimental study was to compare the performance of the three types of reinforcement that had the same characteristics and the same reinforcement material mass. The following is a summary of the results

- An increase in the embedment depth of the footing increased the bearing capacity of the footing on a reinforced slope. Nevertheless, the reinforcement efficiency was less when the footing was placed at a depth of 100 mm rather than at the slope surface. At lower settlement ratios ($s/B \leq$ 4%) for an embedded footing, the geocell reinforcement exhibited significantly higher stiffness, carrying greater loads and experiencing less settlement compared to the planar and wraparound geotextile reinforcements.
- The bearing capacity of the footing increased with an increase in the reinforcement length. The BCR of the reinforcement was found to be directly associated with its length. With an increase in the reinforcement length, the wraparound geotextile exhibited better performance than the planar geotextile and geocell. This indicates that the wraparound geotextile tended to behave better than the planar geotextile because of the confining effect at a sufficient anchorage length of reinforcement. In addition, an increase in the reinforcement length changed the failure mechanism of the reinforced slope. The geocell exhibited better performance for increasing the stiffness and decreasing the horizontal displacement of the slope. The increased length of the other reinforcements was also effective in increasing the stiffness of the slope, resulting in decreases in the horizontal displacement of the slope crest.
- For all reinforcements, reducing the reinforcement spacing from 100 mm to 75 mm enhanced the bearing pressure of the footing and increasing the stiffness of the slope, resulting in reduced deflections. For the 75-mm reinforcement spacing, the geocell reinforcement exhibited significantly higher stiffness, carrying greater loads compared to the planar and wraparound geotextile reinforcements at smaller settlement ratios (s/B ≤ 4%). However, the efficiency of geocell reinforcement was decreased by increasing the settlement ratio because of the larger back length of the planar and wraparound geotextiles compared to the geocell (i.e., L/B = 1.17 and 0.84 for the planar and wraparound geotextile reinforcements and the geocell reinforcement, respectively).
- Increasing in the bearing capacity of footing located on the reinforced slope compared to the unreinforced slope indicated a change in the failure mechanism of the slopes. For the geocell and wraparound geotextile, a reinforcement spacing of 75 mm caused the failure plane to propagate beneath the last layer of the reinforcement. However, by increasing the reinforcement spacing to 100 mm, the failure plane propagated through the interlayer spacing. A local failure mechanism and a local-external failure mechanism were observed for the geocell and wraparound geotextile reinforced slopes, respectively. An internal failure mechanism and persistent tensile cracks were observed for the planar-geotextile reinforced slopes. The footing on the planar-geotextile reinforced slope also experienced more displacement and angular rotation than the other reinforced slopes.

Acknowledgments

The authors would like to acknowledge the financial support provided by Babol Noshirvani University of Technology under grant No. BNUT/395032/00.

References

Adams, M.T. and Collin, J.G. (1997), "Large model spread footing load tests on geosynthetic reinforced soil foundations", *J. Geotech. Geoenviron. Eng.*, **123**(1), 66-72. https://doi.org/10.1061/(ASCE)1090-0241(1997)123:1(66).

Alamshahi, S. and Hataf, N. (2009), "Bearing capacity of strip footings on sand slopes reinforced with geogrid and grid-anchor", *Geotext. Geomembranes*., **27**(3), 217-226. https://doi.org/10.1016/j.geotexmem.2008.11.011.

Ardakani, A. and Namaei, A. (2021), "Numerical investigation of geocell reinforced slopes behavior by considering geocell geometry effect", *Geomech. Eng.*, **24**(6), 589-597. https://doi.org/10.12989/gae.2021.24.6.589.

Ashtiani, M., Ghalandarzadeh, A. and Towhata, I. (2015), "Centrifuge modeling of shallow embedded foundations subjected to reverse fault rupture", *Can. Geotech. J*., **53**(3), 505-519. https://doi.org/10.1139/cgj-2014-0444.

Biswas, S. and Mittal, S. (2017), "Square footing on geocell reinforced cohesionless soils", *Geomech. Eng*., **13**(4), 641-651. https://doi.org/10.12989/gae.2017.13.4.641.

Chen, R. and Chiu, Y. (2008), "Model tests of geocell retaining structures", *Geotext. Geomembranes*, **26**(1), 56-70. https://doi.org/10.1016/j.geotexmem.2007.03.001.

Choudhary, A., Jha, J. and Gill, K. (2010), "Laboratory investigation of bearing capacity behaviour of strip footing on reinforced flyash slope", *Geotext. Geomembranes,* **28**(4), 393-402. https://doi.org/10.1016/j.geotexmem.2009.09.007.

Dash, S.K., Rajagopal, K. and Krishnaswamy, N. (2007), "Behaviour of geocell-reinforced sand beds under strip loading", *Can. Geotech. J*., **44**(7), 905-916. https://doi.org/10.1139/t07-035.

El Sawwaf, M.A. (2007), "Behavior of strip footing on geogrid-reinforced sand over a soft clay slope", *Geotext. Geomembranes,* **25**(1), 50-60. https://doi.org/10.1016/j.geotexmem.2006.06.001.

Fahliani, H.K., Arvin, M.R., Hataf, N. and Khademhosseini, A. (2021), "Experimental Model Studies on Strip Footings Resting on Geocell-Reinforced Sand Slopes", *Int. J. Geosynth. Ground Eng*., **7**(2), 1-15. https://doi.org/10.1007/s40891-021-00270-1.

Hedge, A. and Sitharam, T.G. (2016), "Behaviour of geocell reinforced soft clay bed subjected to incremental cyclic loading", *Geomech. Eng*., **10**(4), 405-422. https://doi.org/10.12989/gae.2016.10.4.405.

Huang, C.C., Tatsuoka, F. and Sato, Y. (1994), "Failure mechanisms of reinforced sand slopes loaded with a footing", *Soils Found.*, **34**(2), 27-40. https://doi.org/10.3208/sandf1972.34.2_27.

Javankhoshdel, S. and Bathurst, R.J. (2017), "Deterministic and

probabilistic failure analysis of simple geosynthetic reinforced soil slopes", *Geosynth. Int.*, **24**(1), 14-29. https://doi.org/10.1680/jgein.16.00012.

Jesmani, M., Kamalzare, M. and Sarbandi, B.B. (2016), "Seismic response of geosynthetic reinforced retaining walls", *Geomech. Eng.*, **10**(5), 635-655. https://doi.org/10.12989/gae.2016.10.5.635.

Kazemian, T. and Arvin, M.R. (2019), "Three-dimensional stability of locally loaded geocell-reinforced slopes by strength reduction method", *Geomech. Geoeng.*, **14**(3), 185-201. https://doi.org/10.1080/17486025.2019.1581275.

Khalaj, O., Tafreshi, S.N.M., Masek, B. and Dawson, A.R. (2015), "Improvement of pavement foundation response with multi layers of geocell reinforcement: Cyclic plate load test", *Geomech. Eng.*, **9**(3), 373-395. https://doi.org/10.12989/gae.2015.9.3.373.

Kumar, A., Singh, P. and Chatterjee, K. (2019), "Ground improvement using geocells to enhance traffic ability in desert soils", *Geomech. Eng.*, **19**(1), 71-78. https://doi.org/10.12989/gae.2019.19.1.071.

Latha, M.G., Dash, S.K. and Rajagopal, K. (2008), "Equivalent continuum simulations of geocell reinforced sand beds supporting strip footings", *Geotech. Geol. Eng.*, **26**(4), 387-398. https://doi.org/10.1007/s10706-008-9176-5.

Latha, M.G., Dash, S.K. and Rajagopal, K. (2009), "Numerical simulation of the behavior of geocell reinforced sand in foundations", *Int. J. Geomech.*, **9**(4), 143-152. https://doi.org10.1061/(ASCE)1532-3641(2009)9:4(143).

Latha, G.M. (2011), "Design of geocell reinforcement for supporting embankments on soft ground", *Geomech. Eng.*, **3**(2), 117-139. https://doi.org/10.12989/gae.2011.3.2.117.

Lee, K. and Manjunath, V. (2000), "Experimental and numerical studies of geosynthetic-reinforced sand slopes loaded with a footing", *Can. Geotech. J.*, **37**(4), 828-842. https://doi.org/10.1139/t00-016.

Mehrjardi, G.T., Ghanbari, A. and Mehdizadeh, H. (2016), "Experimental study on the behaviour of geogrid-reinforced slopes with respect to aggregate size", *Geotext. Geomembranes*, **44**(6), 862-871. https://doi.org/10.1016/j.geotexmem.2016.06.006.

Michalowski, R.L. (1997), "Stability of uniformly reinforced slopes", *J. Geotech. Geoenviron. Eng.*, **123**(6), 546-556. https://doi.org/10.1061/(ASCE)1090-0241(1997)123:6(546).

Pokharel, S.K., Han, J., Leshchinsky, D., Parsons, R.L. and Halahmi, I. (2010), "Investigation of factors influencing behavior of single geocell-reinforced bases under static loading", *Geotext. Geomembranes*, **28**(6), 570-578. https://doi.org/10.1016/j.geotexmem.2010.06.002.

Sarfarazi, V., Tabaroei, A. and Asgari, K. (2022); "Discrete element modeling of strip footing on geogrid-reinforced soil", *Geomech. Eng.*, **29**(4), 435-449. https://doi.org/10.12989/gae.2022.29.4.435.

Saride, S., Pradhan, S., Sitharam, T.G. and Puppala, A.J. (2013), "Numerical analysis of geocell reinforced ballast overlying soft clay subgrade", *Geomech. Eng.*, **5**(3), 263-281. https://doi.org/10.12989/gae.2013.5.3.263.

Sharma, R., Chen, Q., Abu-Farsakh, M. and Yoon, S. (2009), "Analytical modeling of geogrid reinforced soil foundation", *Geotext. Geomembranes*, **27**(1), 63-72. https://doi.org/10.1016/j.geotexmem.2008.07.002.

Song, F., Liu, H.B., Hu, H.B. and Xie, Y.L. (2018a), "Centrifuge tests of geocell-reinforced retaining walls at limit equilibrium", *J. Geotech. Geoenviron. Eng.*, **144**(3), 04018005. https://doi.org/10.1061/(ASCE)GT.1943-5606.0001849.

Song, F., Liu, H.B., Ma, L.Q. and Hu, H.B. (2018b), "Numerical analysis of geocell-reinforced retaining wall failure modes", *Geotext. Geomembranes*, **46**(3), 284-296. https://doi.org/10.1016/j.geotexmem.2018.01.004.

Song, F. and Tian, Y.H. (2019), "Three-dimensional numerical modelling of geocell reinforced soils and its practical application", *Geomech. Eng.*, **17**(1), 1-9. https://doi.org/10.12989/gae.2019.17.1.001.

Song, F., Jin, Y. T., Liu, H.B. and Liu, J. (2020), "Analyzing the deformation and failure of geosynthetic-encased granular soil in the triaxial stress condition", *Geotext. Geomembr Geomembranes*, **48**(6), 886-896. https://doi.org/10.1016/j.geotexmem.2020.06.007.

Song F., Chen W.S., Nie Y.W. and Ma L. Q. (2022), "Evaluation of required stiffness and strength of cellular geosynthetics", *Geosynth. Int.*, **29**(3), 217-228. https://doi.org/10.1680/jgein.21.00032

Tafreshi, S.M. and Dawson, A. (2010), "Comparison of bearing capacity of a strip footing on sand with geocell and with planar forms of geotextile reinforcement", *Geotext. Geomembranes*, **28**(1), 72-84. https://doi.org/10.1016/j.geotexmem.2009.09.003.

Tang, X. and Yang, M. (2013), "Investigation of flexural behavior of geocell reinforcement using three-layered beam model testing", *Geotech. Geol. Eng.*, **31**(2), 753-765. https://doi.org/10.1007/s10706-013-9625-7.

Turker, E., Sadoglu, E., Cure, E. and Uzuner, B.A. (2014), "Bearing capacity of eccentrically loaded strip footings close to geotextile-reinforced sand slope", *Can. Geotech. J.*, **51**(8), 884-895. https://doi.org/10.1139/cgj-2014-0055

Viswanadham, B. and König, D. (2004), "Studies on scaling and instrumentation of a geogrid", *Geotext. Geomembranes*, **22**(5), 307-328. https://doi.org/10.1016/S0266-1144(03)00045-1.

Viswanadham, B. and König, D. (2009), "Centrifuge modeling of geotextile-reinforced slopes subjected to differential settlements", *Geotext. Geomembranes*, **27**(2), 77-88. https://doi.org/10.1016/j.geotexmem.2008.09.008

Won, M.S., Lee, O., Kim, Y.S. and Choi, S. (2016), "An 12 year long term study on the external deformation behavior of Geosynthetic reinforced soil (GRS) walls", *Geomech. Eng.*, **10**(5), 565-575. https://doi.org/10.12989/gae.2016.10.5.565.

Yang, K.H., Zornberg, J., Liu, C.N. and Lin, H.D. (2012), "Stress distribution and development within geosynthetic-reinforced soil slopes", *Geosynth. Int.*, **19**(1), 62-78. https://doi.org/10.1680/gein.2012.19.1.62.

Yazdani, H. and Ashtiani, M. (2022), "Experimental Study on the Effect of Geocell on the Behavior of the Strip Footing Resting on the Soil Slope", *J. Transp. Infra. Eng.*, **8**(3), 91-109. https://doi.org/10.22075/JTIE.2022.27837.1609.

Yoo, C. (2001), "Laboratory investigation of bearing capacity behavior of strip footing on geogrid-reinforced sand slope", *Geotext. Geomembranes*, **19**(5), 279-298. https://doi.org/10.1016/S0266-1144(01)00009-7.

Zhang, L., Zhao, M., Zou, X. and Zhao, H. (2009), "Deformation analysis of geocell reinforcement using Winkler model", *Comput. Geotech.*, **36**(6), 977-983. https://doi.org/10.1016/j.compgeo.2009.03.005.

CC